Unveiling magnetic interactions of ruthenium trichloride via constraining direction of orbital moments: Potential routes to realize a quantum spin liquid

Y. S. Hou, H. J. Xiang,* and X. G. Gong†

Key Laboratory of Computational Physical Sciences (Ministry of Education), State Key Laboratory of Surface Physics, Department of Physics, Fudan University, Shanghai 200433, China

and Collaborative Innovation Center of Advanced Microstructures, Nanjing, 210093, China

(Received 12 October 2016; revised manuscript received 14 May 2017; published 7 August 2017)

Recent experiments reveal that the honeycomb ruthenium trichloride α-$RuCl_3$ is a prime candidate of the Kitaev quantum spin liquid (QSL). However, there is no theoretical model which can properly describe its experimental dynamical response due to the lack of a full understanding of its magnetic interactions. Here, we propose a general scheme to calculate the magnetic interactions in systems (e.g., α-$RuCl_3$) with nonnegligible orbital moments by constraining the directions of orbital moments. With this scheme, we put forward a minimal J_1-K_1-Γ_1-J_3-K_3 model for α-$RuCl_3$ and find that: (I) The third nearest neighbor (NN) antiferromagnetic Heisenberg interaction J_3 stabilizes the zigzag antiferromagnetic order; (II) The NN symmetric off-diagonal exchange Γ_1 plays a pivotal role in determining the preferred direction of magnetic moments and generating the spin wave gap. An exact diagonalization study on this model shows that the Kitaev QSL can be realized by suppressing the NN symmetric off-diagonal exchange Γ_1 and the third NN Heisenberg interaction J_3. Thus, we not only propose a powerful general scheme for investigating the intriguing magnetism of $J_{\text{eff}} = 1/2$ magnets, but also point out future directions for realizing the Kitaev QSL in the honeycomb ruthenium trichloride α-$RuCl_3$.

DOI: 10.1103/PhysRevB.96.054410

I. INTRODUCTION

Quantum spin liquid (QSL) is one of the most exotic and elusive topological states of frustrated magnets showing remarkable collective phenomena, such as emergent gauge fields and fractional particle excitations [1–3]. Of particular interest is the $S = 1/2$ Kitaev model on the honeycomb lattice, which has an exactly solvable QSL ground state [4]. It was proposed that such a model may be realized by the $J_{\text{eff}} = 1/2$ state in the honeycomb iridium oxides, for instance, Na_2IrO_3 and α-Li_2IrO_3 [5–10]. Unfortunately, various experiments show that Na_2IrO_3 has a zigzag antiferromagnetic (AFM) order below 15 K [5,9,10] while α-Li_2IrO_3 has an incommensurate counterrotating magnetic order [11].

Excitingly, some up-to-date experiments [2,12,13] indicate that the honeycomb ruthenium trichloride α-$RuCl_3$ is closer to the Kitaev QSL than the widely studied iridium oxides. It has been demonstrated that α-$RuCl_3$ exhibits frustrated magnetic interactions [12] and can be described by the $J_{\text{eff}} = 1/2$ state [13,14], which is the prerequisite for realizing the Kitaev model. Most importantly, Banerjee *et al.* reported that α-$RuCl_3$ is a proximate Kitaev QSL magnet because its dynamical response measurements above interlayer energy scale are explained in terms of deconfinement physics expected for the QSL [2].

However, a proper theoretical model which could capture its collective magnetic measurements well is still lacking. On one hand, the Heisenberg-Kitaev (HK) model [15,16] cannot account for the experimentally observed magnon gap and the high-energy magnetic mode M_2 [2]. On the other hand, the pure AFM Kitaev model cannot reproduce the experimentally observed concave nature of the edge lower mode in ($\boldsymbol{Q}$, E) space [2,17]. Although experiments showed that α-$RuCl_3$ has a zigzag AFM order below 7 K and its magnetic moments collinearly lie in the $\boldsymbol{ac}$ plane [2,18–20], it is not clear whether the magnetic moments take a direction of 35 or -35° away from the $\boldsymbol{a}$ axis [18]. To address these key questions, the most fundamental issue is to unveil what kinds of magnetic interactions are important in α-$RuCl_3$. Once this issue is pinned down, one can put forward a proper theoretical model to capture the experimental observations and explore how to tune the magnetic interactions so as to experimentally realize the QSL in α-$RuCl_3$.

In this paper, to unveil the magnetic interactions of α-$RuCl_3$, we propose a scheme to extract the magnetic interaction parameters by constraining the directions of orbital moments in the density functional theory (DFT) calculations. Calculations show the magnetic ground state is the zigzag AFM order with magnetic moments along the direction of 35° away from the $\boldsymbol{a}$ axis, in agreement with experiments [2]. Apart from the NN ferromagnetic (FM) Kitaev interaction K_1 and AFM Heisenberg interaction J_1, the NN symmetric off-diagonal exchange Γ_1 and the third NN Heisenberg interaction J_3 and Kitaev interaction K_3 are surprisingly large. In view of such results, we propose a minimal J_1-K_1-Γ_1-J_3-K_3 model. We find that the zigzag AFM order is stabilized by the third NN AFM Heisenberg interaction J_3, and the NN symmetric off-diagonal exchange Γ_1 is of importance to the selection of the preferred direction of magnetic moments and the generation of the spin wave gap. An exact diagonalization study reveals that the Kitaev QSL can be realized by suppressing the NN symmetric off-diagonal exchange Γ_1 and the third NN Heisenberg interaction J_3. We illustrate that our scheme is powerful for studying the magnetism of $J_{\text{eff}} = 1/2$ magnets and sheds light on realizing the Kitaev QSL in α-$RuCl_3$.

*hxiang@fudan.edu.cn
†xggong@fudan.edu.cn

II. COMPUTATIONAL DETAILS

Our first-principles calculations are performed based on the DFT + U method. We use the generalized gradient approximation and the projector-augmented wave (PAW) method with an energy cutoff of 450 eV [21–23]. The on-site repulsion U ranges from 2.5 to 3.5 eV, and the Hund coupling is $J_h = 0.4$ eV [13,24]. Since Ru has a strong spin-orbit coupling (SOC) [2,13,24], SOC is included in our calculations. We adopt the low-temperature monoclinic crystal structure with the space group $C2/m$ [18].

III. CONSTRAINT TO DIRECTION OF ORBITAL MAGNETIC MOMENT OF $J_{\text{eff}} = 1/2$ STATES

The orbital magnetic moment dominates over the spin magnetic moment, and they have the same direction in the $J_{\text{eff}} = 1/2$ state. For the low spin d^5 configuration in the octahedral crystal field, such as Ru^{3+} ion in α-$RuCl_3$ and Ir^{5+} ion in honeycomb Na_2IrO_3, a hole resides in the t_{2g} manifold of d_{xy},d_{yz}, and d_{zx} orbitals. The single ion SOC Hamiltonian $H_{\text{SOC}} = \lambda \mathbf{L}\cdot\mathbf{S}$ entangles the orbital and spin spaces and gives rise to the $J_{\text{eff}} = 1/2$ state [25]

$$\begin{aligned}\left|J_{\text{eff}} = 1/2, j^z_{\text{eff}} = +1/2\right\rangle &= [|d_{xy},\uparrow\rangle + i|d_{zx},\downarrow\rangle + |d_{yz},\downarrow\rangle]/\sqrt{3}, \quad (1a)\\ \left|J_{\text{eff}} = 1/2, j^z_{\text{eff}} = -1/2\right\rangle &= [|d_{xy},\downarrow\rangle + i|d_{zx},\uparrow\rangle - |d_{yz},\uparrow\rangle]/\sqrt{3}. \quad (1b)\end{aligned}$$

Here, $\uparrow$ and $\downarrow$ denote up spin and down spin, respectively. One can obtain based on Eqs. (1a) and (1b) that the total magnetic moment $\langle 2S_z + L_z\rangle$ of the $J_{\text{eff}} = 1/2$ state is 1 μ_B, and it is composed of the dominant orbital moment $2/3\mu_B$ and the spin moment $1/3\mu_B$ [26]. Furthermore, the directions of the former and the latter are the same in any case (see Appendix A). Note that $J_{\text{eff}} = 1/2$ state is distinguished from the atomic $J = 1/2(|\text{L-S}|)$ state with $L = 1$ and $S = 1/2$, which has a total magnetic moment $\pm 1/3$ μ_B with opposite spin and orbital direction [26]. Therefore, it is expected that the orbital magnetic moment has a much more vital effect on the magnetic interaction between two different $J_{\text{eff}} = 1/2$ states.

Here, we demonstrate the directions of orbital moments of α-$RuCl_3$ should be constrained in DFT calculations. Both theoretical and experimental studies have shown that the magnetism of α-$RuCl_3$ is described by the $J_{\text{eff}} = 1/2$ state [2,13,27–30]. Based on the discussion above, it is required that magnetic moments of orbit and spin in α-$RuCl_3$ should point along the same direction in DFT calculations. However, our calculations (see Table I) indicate that the directions of spin and orbital moments of α-$RuCl_3$ will seriously deviate from each other if the directions of the orbital moments are not constrained. Actually, such a deviation also exists in honeycomb Na_2IrO_3 and α-Li_2IrO_3 (see Table I), both of which are also well described by the $J_{\text{eff}} = 1/2$ state [11,31]. The most important reason to result in such a deviation is that, in general, there is only one minimum in nonmagnetic systems, but there may exist many minima in a magnetic system [32]; therefore, spin-polarized DFT calculations do not certainly converge to the accurate magnetic ground state or the desired exited state automatically. Another possible reason is the slight mixing $J_{\text{eff}} = 1/2$ states with $J_{\text{eff}} = 3/2$ states [13] due to the trigonal distortion of the $RuCl_3$ octahedron and the Ru-Ru interactions. Note that such nonnegligible Ru-Ru interactions in the $RuCl_3$ make the potential energy surface complicated and result in many metastable states with misaligned spin and orbital moments. To ensure spin and orbital magnetic moments of the $J_{\text{eff}} = 1/2$ state have the same direction in DFT calculations, we propose constraining the direction of orbital moments. As far as we know, constraining the directions of orbital moments has not been achieved so far, although DFT calculations with the spin moments being constrained along desired directions have been carried out [33,34]. Furthermore, an important utilization of constraining the direction of orbital and spin moments is to extract magnetic interaction parameters because it is necessary to calculate some specific excitation energies of some desired magnetic states with given directions of spin and orbital moments.

Now let us show how the directions of orbital moments can be constrained in the framework of DFT. Actually, constrained DFT in which external constraints are applied in order to simulate excitation processes has been extensively utilized to study magnetism since three decades ago [33,35–38] and was reviewed by Kaduk *et al.* [39] recently. To constrain the direction of orbital moment, we add to the usual DFT total energy a penalty energy E_{constr}

$$E = E_0 + E_{\text{constr}} = E_0 + \sum_t \lambda\left[\mathbf{L}^t_l - \mathbf{L}^{t,0}_l\left(\mathbf{L}^{t,0}_l\cdot\mathbf{L}^t_l\right)\right]^2. \quad (2)$$

Here, E_0 is the usual DFT total energy, $\mathbf{L}^{t,0}_l$ is a unit vector along the desired direction, and $\mathbf{L}^t_l$ is the orbital moment of site

TABLE I. First-principles calculated orbital moments (Cal. Orb. Mom.) and spin moments (Cal. Spin Mom.) in the honeycomb α-$RuCl_3$, Na_2IrO_3, and α-Li_2IrO_3 with only the directions of spin moments being constrained.

		Desired direction			Cal. Orb. Mom. (μ_B)			Cal. Spin Mom. (μ_B)		
Materials	U (eV)	x	y	z	x	y	z	x	y	z
α-$RuCl_3$	2.5	2	2	$\bar{1}$	0.29	0.29	−0.26	0.10	0.10	−0.05
	3.0	2	2	$\bar{1}$	0.33	0.33	−0.11	0.08	0.08	−0.04
	3.5	2	2	$\bar{1}$	0.29	0.29	−0.26	0.06	0.06	−0.03
Na_2IrO_3	3.0	1	1	0	0.30	0.30	−0.06	0.14	0.14	0.00
	3.0	1	1	1	0.27	0.28	0.10	0.11	0.11	0.10
α-Li_2IrO_3	3.0	0	0	1	0.05	0.05	0.33	0.00	0.00	0.06
	3.0	1	1	1	0.34	0.34	0.18	0.22	0.22	0.19

TABLE II. First-principles calculated orbital moments (Cal. Orb. Mom.) and spin moments (Cal. Spin Mom.) in the honeycomb α-$RuCl_3$, Na_2IrO_3, and α-Li_2IrO_3 with the directions of both spin and orbital moments being constrained.

		Desired direction			Cal. Orb. Mom. (μ_B)			Cal. Spin Mom. (μ_B)		
Materials	U (eV)	x	y	z	x	y	z	x	y	z
α-$RuCl_3$	2.5	2	2	$\bar{1}$	0.32	0.32	−0.15	0.10	0.10	−0.05
	3.0	2	2	$\bar{1}$	0.32	0.32	−0.15	0.08	0.08	−0.04
	3.5	2	2	$\bar{1}$	0.35	0.35	−0.17	0.13	0.13	−0.07
Na_2IrO_3	3.0	1	1	0	0.30	0.30	0.00	0.14	0.14	0.00
	3.0	1	1	1	0.24	0.24	0.23	0.12	0.12	0.12
α-Li_2IrO_3	3.0	0	0	1	0.01	0.01	0.34	0.00	0.00	0.05
	3.0	1	1	1	0.20	0.20	0.24	0.10	0.10	0.08

t and angular momentum l (e.g., $l = 2$ for Ru $4d$ orbitals). The parameter λ in units of eV/μ_B^2 is a Lagrange multiplier that controls the penalty energy E_{constr}. This scheme is similar to the method for constraining spin moments proposed by Liu *et al.* [33] and Ma and Dudarev [38]. Here, the Lagrange multiplier λ represents a constraining force or magnetic constraint field applied to the orbital magnetic moments of the (Ru^{3+} in α-$RuCl_3$ or Ir^{5+} in Na_2IrO_3) magnetic ions to keep the system in the desired magnetic direction [37]. We find that, for α-$RuCl_3$, the parameter λ ranging from 0.1 to 1.0 eV/μ_B^2 is sufficient to make the penalty energy E_{constr} less than 10^{-5} eV and satisfactorily constrains the directions of orbital moments (see Table II), and thus, the parameter $\lambda = 0.2\,\mathrm{eV}/\mu_B^2$ is employed in this paper. Note that the directions of spin moment are also constrained in our DFT calculations.

We deduce implementing the abovementioned constraint onto directions of orbital moments into the PAW method in detail. In the PAW method, the all-electron wave function is [40]

$$\Psi(r) = \tilde{\Psi}(r) + \sum_{\Lambda} [\phi_\Lambda(r) - \tilde{\phi}_\Lambda(r)]\langle \tilde{p}_\Lambda | \tilde{\Psi}(r)\rangle. \quad (3)$$

In Eq. (3), $\tilde{\Psi}(r)$ is the pseudowave function, and the index Λ is a shorthand for the atom t, the angular momentum l (e.g., $l = 2$ for Ru $4d$ orbitals in α-$RuCl_3$), the magnetic quantum number m, and the index a, the energy for which Schrödinger's equation is solved. The orbital density matrix is obtained by projection of the crystal wave function onto the augmentation region [41]

$$n^{t,l,\sigma}_{m,m'} = \sum_{n,k} f^{\sigma}_{n,k} \left\langle \Psi^{k,\sigma}_n \middle| P^{t,l}_{m,m'} \middle| \Psi^{k,\sigma}_n \right\rangle. \quad (4)$$

In Eq. (4), t, σ, and n are ion site, spin, and energy band index, respectively. Additionally, m and m' are magnetic quantum numbers, and k is the reciprocal point in the Brillouin zone. Here, $f^{\sigma}_{n,k}$ is the Fermi-Dirac distribution function. The operator $P^{t,l}_{m,m'}$ in Eq. (4) is

$$P^{t,l}_{m,m'} = \theta_{\Omega_t}(r)\delta(|r' - R_t| - |r - R_t|)Y_{lm}(r)Y^*_{lm'}(r'). \quad (5)$$

Using the pseudowave functions, the orbital density matrix is in the form of

$$n^{t,l,\sigma}_{m,m'} = \sum_{n,k} f^{\sigma}_{n,k} \left\langle \tilde{\Psi}^{k,\sigma}_n \middle| \tilde{P}^{t,l}_{m,m'} \middle| \tilde{\Psi}^{k,\sigma}_n \right\rangle. \quad (6)$$

In Eq. (6), the operator $\tilde{P}^{t,l}_{m,m'} = \sum_{\Lambda,\Lambda'} |\tilde{p}_\Lambda\rangle\langle\phi_\Lambda| P^{t,l}_{m,m'} |\phi_{\Lambda'}\rangle\langle\tilde{p}_{\Lambda'}|$. Since spherical harmonics form a complete set of functions, the orbital moment operator $L^{t,\alpha}_l$ for site t and angular momentum l ($\alpha = x, y$, and z) can be computed as

$$\begin{aligned} L^{t,\alpha}_l &= \sum_{n,k,\sigma} f^{k,\sigma}_n \left\langle \Psi^{k,\sigma}_n \middle| \hat{L}^{\alpha} \middle| \Psi^{k,\sigma}_n \right\rangle \\ &= \sum_{n,k,\sigma} f^{k,\sigma}_n \left\langle \Psi^{k,\sigma}_n \middle| \sum_{lm,l'm'} |Y_{lm}\rangle\langle Y_{lm}|\hat{L}^{\alpha}|Y_{l'm'}\rangle \left\langle Y_{l'm'} \middle| \Psi^{k,\sigma}_n \right\rangle \right. \\ &= \sum_{l,m,m',\sigma} L^{\alpha}_{l,mm'} n^{t,l,\sigma}_{m,m'}. \end{aligned} \quad (7)$$

Due to the presence of the additional penalty energy, there is an additional potential

$$\begin{aligned} \hat{H}_L &= \sum_{t,\sigma,\alpha,m,m'} \frac{\partial E}{\partial L^{t,\alpha}_l} \frac{\partial L^{t,\alpha}_l}{\partial n^{t,l,\sigma}_{m,m'}} \frac{\partial n^{t,l,\sigma}_{m,m'}}{\partial \tilde{\rho}_\sigma} \\ &= \sum_{t,\sigma,\alpha,m,m'} \left[2L^{t,\alpha}_l - 2\left(\mathbf{L}^{t,0}_l \cdot \mathbf{L}^{t}_l\right) L^{t,\alpha,0}_l\right] L^{\alpha}_{l,mm'} \tilde{P}^{t,l}_{m,m'}. \end{aligned} \quad (8)$$

In Eq. (8), $\tilde{\rho}_\sigma = \sum_{n,k} f^{\sigma}_{n,k} |\tilde{\Psi}^{k,\sigma}_n\rangle\langle\tilde{\Psi}^{k,\sigma}_n|$ is a two-center pseudodensity matrix operator.

IV. APPLICATION OF CONSTRAINING DIRECTION OF ORBITAL MENTIONS TO QSL CANDIDATE α-$RuCl_3$

We first show the magnetic ground state of α-$RuCl_3$ is the zigzag AFM order with magnetic moments along the direction of 35° away from the $\boldsymbol{a}$ axis. Experiments reveal that α-$RuCl_3$ has a layered honeycomb crystal structure and zigzag AFM order with magnetic moments along a direction of 35 or −35° away from the $\boldsymbol{a}$ axis [18] (Fig. 1). In the (x, y, z) coordinate expressing the HK Hamiltonian [Fig. 1(a)], the directions of 35 and −35° away from the $\boldsymbol{a}$ axis are along the [22$\bar{1}$] and z axes, respectively. Apart from the zigzag AFM order, we examine another three representative magnetic orders, that is, FM [Fig. 2(a)], Néel AFM [Fig. 2(b)], and stripe AFM [Fig. 2(c)]. For each magnetic order, six different directions, namely, x, y, z, $\boldsymbol{a}$, $\boldsymbol{b}$, and [22$\bar{1}$] axes, are taken into account. Shown in Fig. 2(e) are the energy differences between these magnetic orders as a function of U. It is shown that the zigzag AFM order with magnetic moments along the [22$\bar{1}$] axis (denoted as zigzag-22$\bar{1}$, such a denotation method is also

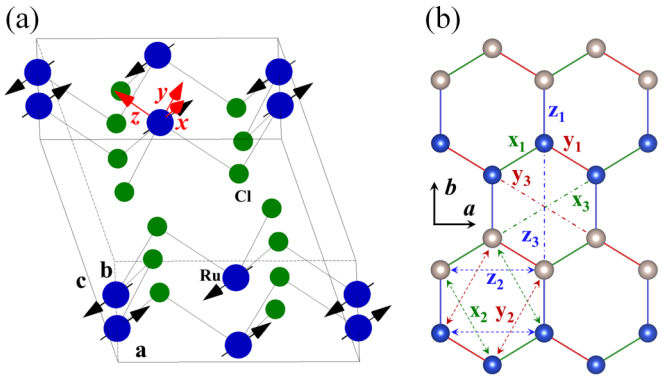

FIG. 1. (a) Crystal structure and zigzag AFM order of α-$RuCl_3$. Ru and Cl atoms are represented by the blue and green spheres, respectively. The (x, y, z) coordinate expressing the HK Hamiltonian is drawn and its x, y, and z axis point along three NN Ru-Cl bonds in a $RuCl_6$ octahedron. Black arrows represent magnetic moments. (b) Magnetic interaction paths. The NN, second NN, and third NN x, y, and z Ru-Ru paths are shown by green, red, and blue lines. Blue and white gray spheres have up and down spins, respectively.

applied to other magnetic orders) has the lowest total energy for all considered U cases, which indicates that the magnetic ground state is the zigzag AFM order with magnetic moments along the direction of 35° away from the $\boldsymbol{a}$ axis and that our scheme works in α-$RuCl_3$.

Having established the magnetic ground state of α-$RuCl_3$, we introduce the Hamiltonian employed in this paper. We

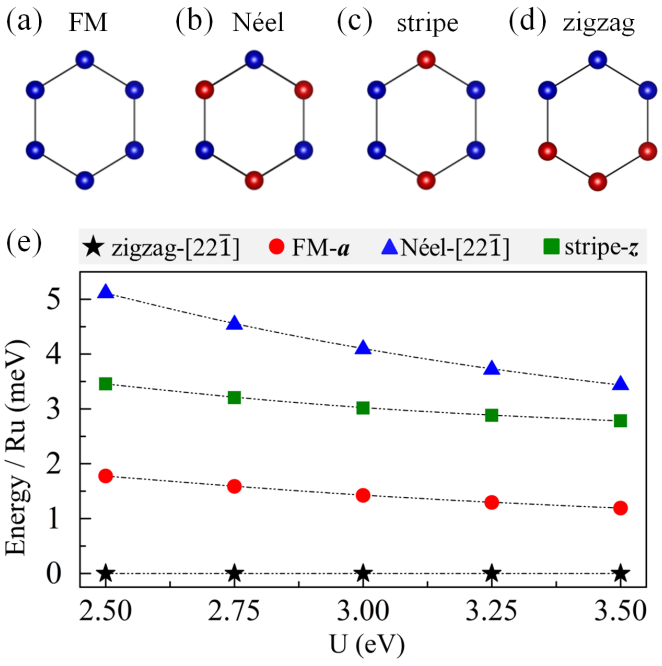

FIG. 2. Illustration of different magnetic orders (a) FM, (b) Néel AFM, (c) stripe AFM, and (d) zigzag AFM. In (a)–(d), blue and red spheres have up and down spins, respectively. (e) Energy differences per Ru atom of the considered magnetic orders are plotted with respect to U. The zigzag-[22$\bar{1}$] (black star) AFM has the lowest energy and is set as the energy reference. As for the FM, Néel AFM, and stripe AFM, only their lowest energies are plotted.

consider a generalized bilinear Hamiltonian widely used in the study of a $J_{\rm eff} = 1/2$ magnet and described as in Refs. [27,42–46], up to the third NN Ru-Ru bonds

$$H = \sum_{ij\in\alpha\beta(\gamma)} \left[J_{ij}\boldsymbol{S}_i\cdot\boldsymbol{S}_j + K_{ij}S_i^\gamma S_j^\gamma + \boldsymbol{D}_{ij}\cdot(\boldsymbol{S}_i\times\boldsymbol{S}_j) + \boldsymbol{S}_i\cdot\boldsymbol{\Gamma}_{ij}\cdot\boldsymbol{S}_j \right], \quad (9)$$

where the last term is the generalized symmetric off-diagonal exchange [46] in the form of

$$\boldsymbol{S}_i\cdot\boldsymbol{\Gamma}_{ij}\cdot\boldsymbol{S}_j = \Gamma_{ij}^x\left(S_i^yS_j^z + S_i^zS_j^y\right) + \Gamma_{ij}^y\left(S_i^zS_j^x + S_i^xS_j^z\right) + \Gamma_{ij}^z\left(S_i^xS_j^y + S_i^yS_j^x\right).$$

In Eq. (9), i and j label Ru sites and $\boldsymbol{S}_i$ is a $J_{\rm eff} = 1/2$ pseudospin operator with components S_i^α ($\alpha = x,y,z$). Parameters J_{ij}, K_{ij}, and $\boldsymbol{D}_{ij}$ are the Heisenberg, Kitaev, and Dzyaloshinskii-Moriya (DM) interactions, respectively. Every Ru-Ru bond ij is distinguished by one spin direction γ [Fig. 1(b)] and another two directions α and β [46].

Here, α-$RuCl_3$ has the dominating NN FM Kitaev interaction and sizable NN symmetric off-diagonal exchange. Shown in the Table III are the calculated magnetic interaction parameters by means of the four-states method [47]. Although the magnitudes of magnetic interaction parameters are U dependent (see Appendix B), the NN x, y, and z bonds have FM Heisenberg interactions and dominating FM Kitaev interactions. Note that the NN FM Kitaev interaction is consistent with the recent theoretical results obtained by the nonperturbative exact diagonalization methods [45] and by quantum chemistry calculations [48]. In contrast to our results, the NN Kitaev interaction is estimated to be AFM with the perturbation theory in which tight binding parameters are deduced from the *ab initio* calculations [27]. Furthermore, the NN symmetric off-diagonal exchange is sizable and bond dependent. For example, the NN z bond has the sizable Γ^z component, while the other two components Γ^x and Γ^y are negligible. Unexpectedly, the second NN magnetic interactions are relatively much weak. However, the third NN Ru-Ru bonds have weak AFM Kitaev interactions and sizable AFM Heisenberg interactions comparable to the NN FM Heisenberg interactions, which are different from the Na_2IrO_3 case, where the second and third NN Heisenberg interactions are both estimated to be comparable to the NN Heisenberg interaction [5]. Lastly, the DM interactions are all negligible because of the quasi-inversion symmetry of the Ru_2Cl_{10} cluster.

Based on our calculated magnetic interaction parameters, we propose that the minimal model of α-$RuCl_3$ is the J_1-K_1-Γ_1-J_3-K_3 one

$$H = \sum_{\langle ij\rangle\in\alpha\beta(\gamma)} \left[J_1\boldsymbol{S}_i\cdot\boldsymbol{S}_j + K_1S_i^\gamma S_j^\gamma + \Gamma_1\left(S_i^\alpha S_j^\beta + S_i^\beta S_j^\alpha\right)\right] + \sum_{\langle\langle\langle ij\rangle\rangle\rangle\in\alpha\beta(\gamma)} \left(J_3\boldsymbol{S}_i\cdot\boldsymbol{S}_j + K_3S_i^\gamma S_j^\gamma\right). \quad (10)$$

Here, the second NN magnetic interactions are left out of consideration as they are weak compared with the NN and third NN magnetic interactions. For simplicity, the NN (third NN) x, y, and z bonds are considered to be equivalent since

TABLE III. Calculated magnetic interaction parameters in units of meV in the case of different U. Detailed magnetic interaction parameters are given in the Appendix B. The letters x, y, and z in parentheses are the indicator of Ru-Ru bonds. The last row is the magnetic interaction parameters of the J_1-K_1-Γ_1-J_3-K_3 model.

U (eV)	$J_1(z)$	$J_1(x/y)$	$K_1(z)$	$K_1(x/y)$	$\Gamma_1^z(z)$	$\Gamma_1^{x/y}(x/y)$	$J_3(z)$	$J_3(x/y)$	$K_3(z)$	$K_3(x/y)$
2.5	−2.1	−2.5	−13.9	−14.7	6.5	6.4	2.0	2.1	0.9	0.9
3.0	−1.8	−2.2	−11.9	−12.4	4.9	4.8	1.6	1.6	0.8	0.7
3.5	−1.6	−2.0	−10.4	−10.8	3.8	3.8	1.2	1.3	0.7	0.6

Model	J_1	K_1	Γ_1	J_3	K_3
	−1.8	−10.6	3.8	1.25	0.65

they have similar magnetic interactions. The magnitudes of parameters J_1, K_1, Γ_1, J_3, and K_3, listed in the last row in the Table III, are obtained by averaging the corresponding results calculated based on the $U = 3.5$ eV.

The experimentally observed zigzag AFM structure is well reproduced by the J_1-K_1-Γ_1-J_3-K_3 model. The efficient exchange Monte Carlo (MC) [49–51] simulation indicates the magnetic ground state is the zigzag AFM order with magnetic moments along the $[77\bar{2}]$ direction which is 43° (close to the experimentally observed 35°) away from the $\boldsymbol{a}$ axis. In addition, MC simulations reveal that the magnetic transition temperature is 8.8 K, quite closed to the experimentally measured $T_N = 7$ K [18].

The third NN AFM Heisenberg interaction and the NN symmetric off-diagonal exchange play an important role in establishing the experimentally observed zigzag AFM structure. If only the dominating NN FM Kitaev interaction K_1 and the NN FM Heisenberg interaction J_1 are considered, the magnetic ground state is at the boundary of the Kitaev QSL [52]. However, MC simulations show that such a proximate Kitaev QSL breaks down, and the zigzag AFM order stabilizes, provided that the third NN AFM Heisenberg interaction J_3 is additionally included. Such a simulated result is reasonable because the third NN AFM Heisenberg interaction J_3 is magnetically satisfied in the zigzag AFM order [Fig. 1(b)]. Based on such a zigzag AFM order, extra MC simulations, including the NN symmetric off-diagonal exchange Γ_1, show that the magnetic ground state is the $[77\bar{2}]$ oriented zigzag AFM order. Further MC simulations indicate such a zigzag AFM order is robust and not destroyed by the third NN AFM Kitaev interaction K_3.

The NN symmetric off-diagonal exchange and the NN FM Kitaev interaction cooperatively determine the preferred direction of magnetic moments of the zigzag AFM order. Obviously, the preferred direction is determined by the anisotropic Kitaev interaction and symmetric off-diagonal exchange. To make clear how it is picked out by them, we assume magnetic moments are parallel or antiparallel to the arbitrary unit vector $e_{xyz} = (xyz)$ in the (x, y, z) coordinate. Then the dependence of the energy on the vector e_{xyz} is

$$E = 2J_1 - 6J_3 + 2K_1(x^2 + y^2 - z^2) - 2K_3 - 4\Gamma_1(xy - yz - zx). \quad (11)$$

Equation (11) clearly indicates the preferred direction is determined by the NN symmetric off-diagonal exchange Γ_1 and the NN FM Kitaev interaction K_1. Surprisingly, the third NN AFM Kitaev interaction K_3 makes no contribution to determining the preferred direction. If the symmetric off-diagonal exchange Γ_1 is only taken into account, the zigzag AFM order prefers being along the optimal [111] direction. Similarly, the zigzag order AFM order prefers lying in the xy plane if only the NN FM Kitaev interaction K_1 is considered. If both are taken into consideration, the zigzag AFM order prefers being along the optimal $[77\bar{2}]$ direction.

The experimentally measured dynamical response is captured by the J_1-K_1-Γ_1-J_3-K_3 model. Shown in Fig. 3(a) is the linear spin wave theory (LSWT) calculated spin wave spectrum. This spectrum has a minimum 2.22 meV in the vicinity of the $\mathbf{M} = (0.5\,0.5\,0.0)$ point, which is consistent with the fact that the experimentally measured low-energy magnetic mode M_1 has structured scattering near $Q = 0.62$ Å^{-1} at the lowest-energy 2.25 meV [2]. More importantly, the LSWT calculated powder-averaged scattering captures the experimentally observed magnetic modes M_1 and M_2 [Fig. 3(b)]. The calculated energy positions of the low-energy magnetic mode M_1 and the high-energy magnetic mode M_2 locate at $E_1 = 5.0$ meV and $E_2 = 6.6$ meV, respectively, which are consistent with the experimentally measured $E_1 = 4.1$ meV and $E_2 = 6.5$ meV [2]. Additionally, the experimentally observed concave nature of the edge of the lower mode in ($\boldsymbol{Q}$, E) space is reproduced [Fig. 3(b)]. Further study shows, if the NN symmetric off-diagonal exchange Γ_1 is slightly renormalized to 3.0 from 3.8 meV, the spin wave spectrum will have a minimum 2.41 meV near the $\mathbf{M}$ point and the E_1 of the M_1 mode and the E_2 of the M_2 mode will be 4.3 and 6.3 meV, respectively. These are very close to the experimental observations. Hence,

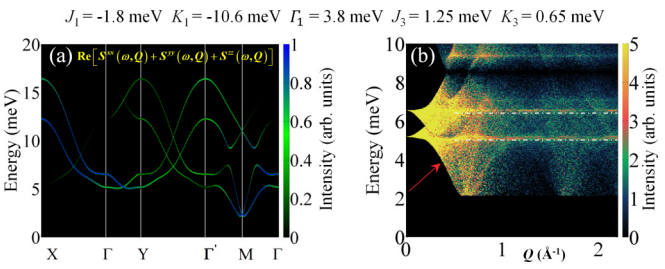

FIG. 3. (a) Spin-wave spectrum and (b) powder-averaged scattering of the J_1-K_1-Γ_1-J_3-K_3 model calculated with the LSWT. The adopted magnetic interaction parameters are listed in the legend. In (b), the red arrow highlights the experimentally observed concave nature of the edge of the lower mode in ($\boldsymbol{Q}$, E) space [2], and the white dash-dotted lines show the energy positions of the magnetic modes M_1 and M_2.

the J_1-K_1-Γ_1-J_3-K_3 model nicely captures the dynamical response measurements of α-$RuCl_3$.

The NN symmetric off-diagonal exchange is central to the presence of the spin wave gap. Here, the $[77\bar{2}]$ direction is approximated by the [110] one for simplicity, and we consider two points in the reciprocal space, the $\Gamma = (0.0\,0.0\,0.0)$ point and the $\mathbf{M} = (0.5\,0.5\,0.0)$ point. At the Γ point, LSWT predicts four branches of energy (see Appendix C)

$$E_1^\Gamma = \sqrt{\Gamma_1(\Gamma_1 + 2J_1 + 6J_3 + 2K_3)/2}, \tag{12a}$$

$$E_2^\Gamma = \sqrt{(J_1 + 3J_3 + K_3)(\Gamma_1 - 2K_1)/2}, \tag{12b}$$

$$E_3^\Gamma = \sqrt{(\Gamma_1 - 2J_1 + 6J_3 + 2K_3)(\Gamma_1 - 2J_1 - K_1)/2}, \tag{12c}$$

$$E_4^\Gamma = \sqrt{(J_1 - 3J_3 - K_3 + K_1)(4J_1 - \Gamma_1 + 2K_1)/2}. \tag{12d}$$

At the $\mathbf{M}$ point, LSWT predicts two doubly degenerate energies (see Appendix C), and the lowest one of them is

$$E_1^M = E_2^M = \tfrac{1}{2}\sqrt{-{\Gamma_1}^2 - \Gamma_1(J_1 - 3J_3 - K_3 + K_1) + {K_1}^2 + J_1K_1 - 3J_3K_1 - K_1K_3 - \Delta}. \tag{13}$$

In Eq. (13), the parameter Δ is dependent on the Heisenberg, Kitaev interactions, and off-diagonal exchange (see Appendix C). Equations (12a) and (13) show that energies E_1^Γ and E_1^M (E_2^M) are zero in the absence of the NN symmetric off-diagonal exchange Γ_1, indicating that the spin wave spectrum inevitably has no gap. Such a nongapped spin wave spectrum is consistent with the theoretical results of Banerjee *et al.* [2] since no symmetric off-diagonal exchange is included in their Hamiltonian. Therefore, the NN symmetric off-diagonal exchange is necessary to the presence of a spin wave gap.

Here, we discuss how the Kitaev QSL can be realized in α-$RuCl_3$ in future experiments. If only the NN Kitaev interactions K_1 and Heisenberg interaction J_1 are taken into consideration, an exact diagonalization study on a 24-site cluster shows the Kitaev QSL survives in a window from $J_1/|K_1| = -0.17$ to $J_1/|K_1| = 0.12$ around the exact Kitaev point [Fig. 4(a)] [52]. The ratio of $J_1/|K_1|$ in the J_1-K_1-Γ_1-J_3-K_3 model is -0.1698, indicating that α-$RuCl_3$ has the Kitaev QSL ground state. Further study shows that such a state persists even though the third NN Kitaev interaction K_3 is involved [Fig. 4(b)]. However, the Kitaev QSL breaks down if either the NN symmetric off-diagonal exchange Γ_1 or the third NN Heisenberg interaction J_3 is further considered [Figs. 4(c) and 4(d)]. Especially, the Kitaev QSL is fragile against the NN symmetric off-diagonal exchange Γ_1. This paper indicates that it is crucial to weaken the NN symmetric off-diagonal exchange Γ_1 and the third NN Heisenberg interaction J_3 to realize the Kitaev QSL in α-$RuCl_3$ in future experiments. Such weakening may be achieved by applying strain, hydrostatic pressure, isovalent ion doping, etc.

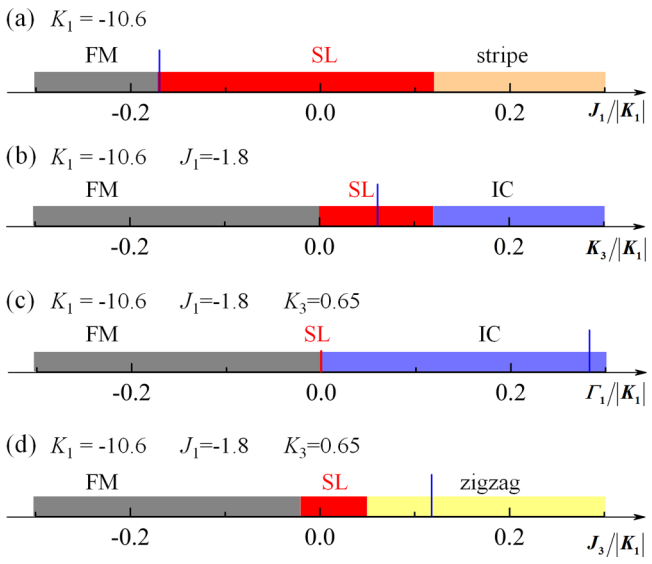

FIG. 4. By turning on the different magnetic interactions in the minimal J_1-K_1-Γ_1-J_3-K_3 model, we explore based on the exact diagonalization study the breakdown of the Kitaev QSL due to (a) the NN Heisenberg interaction J_1, (b) the third NN Kitaev coupling K_3, (c) the NN symmetric off-diagonal exchange Γ_1 (3.0 meV is adopted here), and (d) the third NN Heisenberg interaction J_3. SL and IC denote "spin liquid" and "incommensurate", respectively. The magnetic parameters shown in the legend are in units of meV. The blue vertical lines in (a)–(d) show the ratio $J_1/|K_1|, K_3/|K_1|, \Gamma_1/|K_1|$, and $J_3/|K_1|$, respectively, which are calculated based on the magnetic interactions parameters listed in the last row in Table III.

V. SUMMARY

In summary, to understand the nature of the proximate Kitaev QSL in α-$RuCl_3$, we propose a method to extract the magnetic interaction parameters in the spin-orbit coupled systems by constraining the direction of orbital moments. With this method, we have successfully unveiled the magnetic interactions of α-$RuCl_3$ and thus propose a minimal J_1-K_1-Γ_1-J_3-K_3 model which captures the experimental observations well. Since the NN Kitaev interaction K_1 remarkably dominates over other kinds of magnetic interactions, α-$RuCl_3$ should be proximate to the Kitaev QSL. Importantly, we propose the Kitaev QSL could be realized by suppressing the NN symmetric off-diagonal exchange and the third NN Heisenberg interaction. We demonstrate the present scheme is efficient for studying the magnetism of $J_{\text{eff}} = 1/2$ magnets and give hints to future experiments for realizing the Kitaev QSL in α-$RuCl_3$.

ACKNOWLEDGMENTS

This paper was partially supported by the National Natural Science Foundation of China, the Special Funds for Major State Basic Research (Grant No. 2015CB921700), Program for Professor of Special Appointment (Eastern Scholar), Qing Nian Ba Jian Program, and Fok Ying Tung Education Foundation. We thank Y. L. Zhang and J. S. Feng for useful discussions.

TABLE IV. First-principles calculated magnetic interaction parameters (in meV) of Hamiltonian Eq. (9) (see the main text) in the case of $U = 2.5$ eV. NN, NNN, and NNNN denote the nearest neighbor, next nearest neighbor, and third nearest neighbor, respectively.

$U = 2.5$		J	K	Γ^x	Γ^y	Γ^z	$\boldsymbol{D}^x$	$\boldsymbol{D}^y$	$\boldsymbol{D}^z$
NN	z	−2.06	−13.92	−0.17	−0.18	6.50	−0.02	0.00	0.00
	x/y	−2.53	−14.68	6.35	−0.19	−0.13	0.03	−0.01	0.00
NNN	z	0.38	−0.40	0.38	0.30	0.39	0.18	0.46	0.37
	x/y	0.74	−0.23	0.34	0.40	0.28	−0.25	−0.45	−0.41
NNNN	z	2.04	0.87	−0.19	−0.08	−0.18	−0.03	−0.01	0.05
	x/y	2.09	0.87	−0.23	−0.23	−0.03	0.05	−0.07	0.02

APPENDIX A: PROOF OF THE SAME DIRECTION OF SPIN AND ORBITAL MOMENTS IN THE $J_{\text{eff}} = 1/2$ STATE

We show that, in the $J_{\text{eff}} = 1/2$ state, the spin and orbital moments have the same direction in any case. The $J_{\text{eff}} = 1/2$ state is cast in the form of

$$|\Uparrow\rangle = \left|J_{\text{eff}} = 1/2, j^z_{\text{eff}} = +1/2\right\rangle = [|d_{xy},\uparrow\rangle + i|d_{zx},\downarrow\rangle + |d_{yz},\downarrow\rangle]/\sqrt{3}, \quad \text{(A1a)}$$

$$|\Downarrow\rangle = \left|J_{\text{eff}} = 1/2, j^z_{\text{eff}} = -1/2\right\rangle = [|d_{xy},\downarrow\rangle + i|d_{zx},\uparrow\rangle - |d_{yz},\uparrow\rangle]/\sqrt{3}. \quad \text{(A1b)}$$

In the basis of $|\Uparrow\rangle$ and $|\Downarrow\rangle$, the matrices of spin angular momenta operator $\boldsymbol{S}$, the orbital angular momenta operator $\boldsymbol{L}$, and total angular momenta operator $\boldsymbol{J} = \boldsymbol{S} - \boldsymbol{L}$ are in the form of

$$S_x = \frac{1}{6}\begin{bmatrix}0 & 1\\ 1 & 0\end{bmatrix} \quad S_y = \frac{1}{6}\begin{bmatrix}0 & -i\\ i & 0\end{bmatrix} \quad S_z = \frac{1}{6}\begin{bmatrix}-1 & 0\\ 0 & 1\end{bmatrix}, \quad \text{(A2a)}$$

$$L_x = \frac{2}{3}\begin{bmatrix}0 & 1\\ 1 & 0\end{bmatrix} \quad L_y = \frac{2}{3}\begin{bmatrix}0 & -i\\ i & 0\end{bmatrix} \quad L_z = \frac{2}{3}\begin{bmatrix}-1 & 0\\ 0 & 1\end{bmatrix}, \quad \text{(A2b)}$$

$$J_x = \frac{1}{2}\begin{bmatrix}0 & -1\\ -1 & 0\end{bmatrix} \quad J_y = \frac{1}{2}\begin{bmatrix}0 & i\\ -i & 0\end{bmatrix} \quad J_z = \frac{1}{2}\begin{bmatrix}1 & 0\\ 0 & -1\end{bmatrix}. \quad \text{(A2c)}$$

Comparing Eq. (A2b) with stand Pauli matrices of the spin-1/2, we can find that the $J_{\text{eff}} = 1/2$ state is an analogue to spin-1/2. Note that, in the Pauli matrices, the arbitrary quantum phase α is set to be zero [53], but it is π for the $J_{\text{eff}} = 1/2$ state. For arbitrary normalized state $|\varphi\rangle = C_1|\Uparrow\rangle + C_2|\Downarrow\rangle$, the magnetic moments of $\boldsymbol{S}$ and $\boldsymbol{L}$ are

$$M_{\boldsymbol{S}} = 2\langle\varphi|\boldsymbol{S}|\varphi\rangle = \tfrac{1}{3}\left[C_1C_2^\dagger + C_1^\dagger C_2 \quad i(C_1C_2^\dagger - C_1^\dagger C_2) \quad C_2^2 - C_1^2\right], \quad \text{(A3a)}$$

$$M_{\boldsymbol{L}} = \langle\varphi|\boldsymbol{L}|\varphi\rangle = \tfrac{2}{3}\left[C_1C_2^\dagger + C_1^\dagger C_2 \quad i(C_1C_2^\dagger - C_1^\dagger C_2) \quad C_2^2 - C_1^2\right]. \quad \text{(A3b)}$$

From Eqs. (A3a) and (A3b), one can obtain that the magnetic moments of $\boldsymbol{S}$ and $\boldsymbol{L}$, which have the same direction.

APPENDIX B: DETAILED MAGNETIC INTERACTION PARAMETERS OF α-$RuCl_3$ IN THE CASE OF DIFFERENT U

The magnetic interaction parameters of the generalized bilinear Hamiltonian, Eq. (9), of α-$RuCl_3$ are given at length in the Table IV ($U = 2.5$ eV), Table V ($U = 3.0$ eV), and Table VI ($U = 3.5$ eV).

APPENDIX C: LSWT ANALYSIS OF THE J_1-K_1-Γ_1-J_3-K_3 HAMILTONIAN

The J_1-K_1-Γ_1-J_3-K_3 Hamiltonian takes the form of

$$H = \sum_{\langle ij\rangle\in\alpha\beta(\gamma)}\left[\left(J_1\boldsymbol{S}_i\cdot\boldsymbol{S}_i + K_1S_i^\gamma S_j^\gamma\right) + \Gamma_1\left(S_i^\alpha S_j^\beta + S_i^\beta S_j^\alpha\right)\right] + \sum_{\langle\langle\langle ij\rangle\rangle\rangle\in\alpha\beta(\gamma)}\left(J_3\boldsymbol{S}_i\cdot\boldsymbol{S}_i + K_3S_i^\gamma S_j^\gamma\right). \quad \text{(C1)}$$

Here, we consider the zigzag AFM order in the magnetic unit cell containing four magnetic ions and set lattice constants $\boldsymbol{a}$ and $\boldsymbol{b}$ as 1. Note that the magnetic moments are along the [110] direction in the (x, y, z) coordinate system explicitly given in the main text. Under the basis

TABLE V. First-principles calculated magnetic interaction parameters (in meV) of Hamiltonian Eq. (9) (see the main text) in the case of $U = 3.0$ eV.

$U = 3.0$		J	K	Γ^x	Γ^y	Γ^z	$\boldsymbol{D}^x$	$\boldsymbol{D}^y$	$\boldsymbol{D}^z$
NN	z	−1.78	−11.86	−0.22	−0.22	4.92	−0.03	0.03	0.01
	x/y	−2.21	−12.38	4.84	−0.25	−0.20	−0.01	−0.02	0.03
NNN	z	0.29	−0.31	0.28	0.24	0.31	0.10	0.32	0.21
	x/y	0.55	−0.07	0.29	0.29	0.23	−0.19	−0.32	−0.25
NNNN	z	1.55	0.81	−0.16	0.03	−0.16	0.00	0.02	0.01
	x/y	1.61	0.73	−0.10	−0.17	−0.01	0.10	−0.03	−0.01

TABLE VI. First-principles calculated magnetic interaction parameters (in meV) of Hamiltonian Eq. (9) (see the main text) in the case of $U = 3.5$ eV.

$U = 3.5$		J	K	Γ^x	Γ^y	Γ^z	$\boldsymbol{D}^x$	$\boldsymbol{D}^y$	$\boldsymbol{D}^z$
NN	z	−1.63	−10.35	−0.22	−0.22	3.79	−0.02	0.02	−0.07
	x/y	−2.01	−10.76	3.84	−0.25	−0.28	−0.02	−0.01	−0.07
NNN	z	0.23	−0.24	0.22	0.17	0.31	0.05	0.22	0.23
	x/y	0.23	−0.03	0.23	0.23	0.26	−0.13	−0.24	−0.13
NNNN	z	1.22	0.67	−0.12	0.02	−0.20	0.00	0.00	−0.06
	x/y	1.27	0.63	−0.14	−0.12	−0.03	0.02	0.01	−0.07

$\mathbf{x}(\mathbf{k}) = [b_1(\mathbf{k}), b_2(\mathbf{k}), b_3(\mathbf{k}), b_4(\mathbf{k}), b_1{}^+(-\mathbf{k}), b_2{}^+(-\mathbf{k}), b_3{}^+(-\mathbf{k}), b_4{}^+(-\mathbf{k})]$, the matrix form of the Hamiltonian Eq. (C1) is [54]

$$H = \begin{bmatrix} A(\boldsymbol{k}) - C(\boldsymbol{k}) & B(\boldsymbol{k}) \\ B^\dagger(\boldsymbol{k}) & A(-\boldsymbol{k}) - C(\boldsymbol{k}) \end{bmatrix}. \tag{C2}$$

In Eq. (C2), $A(\boldsymbol{k})$, $A(-\boldsymbol{k})$, $B(\boldsymbol{k})$, and $C(\boldsymbol{k})$ are four-by-four matrices, and their explicit expressions are as follows:

$$A(\boldsymbol{k}) = \begin{bmatrix} 0 & 0 & A(\boldsymbol{k})^{1,3} & A(\boldsymbol{k})^{1,4} \\ 0 & 0 & A(\boldsymbol{k})^{2,3} & A(\boldsymbol{k})^{2,4} \\ \overline{A(\boldsymbol{k})^{1,3}} & \overline{A(\boldsymbol{k})^{1,4}} & 0 & 0 \\ \overline{A(\boldsymbol{k})^{2,3}} & \overline{A(\boldsymbol{k})^{2,4}} & 0 & 0 \end{bmatrix}, \tag{C3a}$$

$$A(-\boldsymbol{k}) = \begin{bmatrix} 0 & 0 & A(-\boldsymbol{k})^{1,3} & A(-\boldsymbol{k})^{1,4} \\ 0 & 0 & A(-\boldsymbol{k})^{2,3} & A(-\boldsymbol{k})^{2,4} \\ \overline{A(-\boldsymbol{k})^{1,3}} & \overline{A(-\boldsymbol{k})^{1,4}} & 0 & 0 \\ \overline{A(-\boldsymbol{k})^{2,3}} & \overline{A(-\boldsymbol{k})^{2,4}} & 0 & 0 \end{bmatrix}, \tag{C3b}$$

$$B(\boldsymbol{k}) = \begin{bmatrix} 0 & 0 & B(\boldsymbol{k})^{1,3} & B(\boldsymbol{k})^{1,4} \\ 0 & 0 & B(\boldsymbol{k})^{2,3} & B(\boldsymbol{k})^{2,4} \\ B(\boldsymbol{k})^{3,1} & B(\boldsymbol{k})^{3,2} & 0 & 0 \\ B(\boldsymbol{k})^{4,1} & B(\boldsymbol{k})^{4,2} & 0 & 0 \end{bmatrix}, \tag{C3c}$$

$$C(\boldsymbol{k}) = \begin{bmatrix} C & 0 & 0 & 0 \\ 0 & C & 0 & 0 \\ 0 & 0 & C & 0 \\ 0 & 0 & 0 & C \end{bmatrix}. \tag{C3d}$$

The nonvanishing matrix elements are

$$A(\boldsymbol{k})^{1,3} = \frac{1}{4}\left\{-(\Gamma_1 + K_1)e^{-i2\pi k_b} + \frac{K_3}{2}[e^{i2\pi(k_a - k_b)} + e^{-i2\pi(k_a + k_b)} - 2]\right\},$$

$$B(\boldsymbol{k})^{1,3} = \frac{1}{4}\{(2J_1 - \Gamma_1 + K_1)e^{-i2\pi k_b} + 2J_3[1 + e^{-i2\pi(k_a + k_b)} + e^{i2\pi(k_a - k_b)}]\} + \frac{1}{4} \times \frac{K_3}{2}[e^{i2\pi(k_a - k_b)} + e^{-i2\pi(k_a + k_b)} + 2],$$

$$B(\boldsymbol{k})^{3,1} = \frac{1}{4}\{(2J_1 - \Gamma_1 + K_1)e^{i2\pi k_b} + 2J_3[1 + e^{i2\pi(k_a + k_b)} + e^{i2\pi(-k_a + k_b)}]\} + \frac{1}{4} \times \frac{K_3}{2}[e^{i2\pi(-k_a + k_b)} + e^{i2\pi(k_a + k_b)} + 2],$$

$$A(\boldsymbol{k})^{1,4} = \frac{1}{4}\left(2J_1 + \frac{K_1}{2}\right)(1 + e^{i2\pi k_a}),$$

$$B(\boldsymbol{k})^{1,4} = \frac{1}{4}\left(\frac{K_1}{2} - i\sqrt{2}\Gamma_1\right)e^{i2\pi k_a} + \frac{1}{4}\left(\frac{K_1}{2} + i\sqrt{2}\Gamma_1\right),$$

$$B(\boldsymbol{k})^{4,1} = \frac{1}{4}\left(\frac{K_1}{2} - i\sqrt{2}\Gamma_1\right)e^{-i2\pi k_a} + \frac{1}{4}\left(\frac{K_1}{2} + i\sqrt{2}\Gamma_1\right),$$

$$A(\boldsymbol{k})^{2,3} = \frac{1}{4}\left(2J_1 + \frac{K_1}{2}\right)(1 + e^{-i2\pi k_a}),$$

$$B(\boldsymbol{k})^{2,3} = \frac{1}{4}\left(\frac{K_1}{2} - i\sqrt{2}\Gamma_1\right)e^{-i2\pi k_a} + \frac{1}{4}\left(\frac{K_1}{2} + i\sqrt{2}\Gamma_1\right),$$

$$B(\boldsymbol{k})^{3,2} = \frac{1}{4}\left(\frac{K_1}{2} - i\sqrt{2}\Gamma_1\right)e^{i2\pi k_a} + \frac{1}{4}\left(\frac{K_1}{2} + i\sqrt{2}\Gamma_1\right),$$

$$A(\boldsymbol{k})^{2,4} = \frac{1}{4}\{-(\Gamma_1 + K_1) + K_3[\cos(2\pi k_a) - e^{i2\pi k_b}]\},$$

$$B(\boldsymbol{k})^{2,4} = \frac{1}{4}\{(2J_1 - \Gamma_1 + K_1) + 2J_3[e^{i2\pi k_b} + 2\cos(2\pi k_a)] + K_3[\cos(2\pi k_a) + e^{i2\pi k_b}]\},$$

$$B(\boldsymbol{k})^{4,2} = \frac{1}{4}\{(2J_1 - \Gamma_1 + K_1) + 2J_3[e^{-i2\pi k_b} + 2\cos(2\pi k_a)] + K_3[\cos(2\pi k_a) + e^{-i2\pi k_b}]\},$$

$$C = \frac{1}{2}(J_1 + K_1 - \Gamma_1 - 3J_3 - K_3).$$

Based on the above formulas, we find that the four spin wave branch energies at the Γ point (0.0 0.0 0.0) are

$$E_1^{\Gamma} = \sqrt{\Gamma_1(\Gamma_1 + 2J_1 + 6J_3 + 2K_3)/2}, \tag{C4a}$$

$$E_2^{\Gamma} = \sqrt{(J_1 + 3J_3 + K_3)(\Gamma_1 - 2K_1)/2}, \tag{C4b}$$

$$E_3^{\Gamma} = \sqrt{(\Gamma_1 - 2J_1 + 6J_3 + 2K_3)(\Gamma_1 - 2J_1 - K_1)/2}, \tag{C4c}$$

$$E_4^{\Gamma} = \sqrt{(J_1 - 3J_3 - K_3 + K_1)(4J_1 - \Gamma_1 + 2K_1)/2}. \tag{C4d}$$

Likewise, the four spin wave branch energies at the **M** point (0.5 0.5 0.0) are

$$E_1 = E_2 = \frac{1}{2}\sqrt{-{\Gamma_1}^2 - \Gamma_1(J_1 - 3J_3 - K_3 + K_1) + {K_1}^2 + J_1K_1 - 3J_3K_1 - K_1K_3 - \Delta}, \tag{C5a}$$

$$E_3 = E_4 = \frac{1}{2}\sqrt{-{\Gamma_1}^2 - \Gamma_1(J_1 - 3J_3 - K_3 + K_1) + {K_1}^2 + J_1K_1 - 3J_3K_1 - K_1K_3 + \Delta}. \tag{C5b}$$

In Eqs. (C5a) and (C5b), the parameter Δ is as follows:

$$\Delta = \sqrt{\begin{array}{l}\Gamma_1^4 - 2\Gamma_1^3(5J_1 - 15J_3 + 4K_1 - 5K_3) \\ \quad +\Gamma_1^2\left[9J_1^2 - 6J_1(9J_3 - K_1 + 3K_3) + 81{J_3}^2 - 2K_1^2 + 9K_3^2 - 18J_3K_1 + 54J_3K_3 - 6K_1K_3\right] \\ \quad +2\Gamma_1K_1(J_1 - 3J_3 - K_3)(J_1 - 3J_3 - K_3 + K_1) + K_1^2(J_1 - 3J_3 - K_3 + K_1)^2.\end{array}}$$

[1] L. Balents, Nature **464**, 199 (2010).

[2] A. Banerjee, C. A. Bridges, J.-Q. Yan, A. A. Aczel, L. Li, M. B. Stone, G. E. Granroth, M. D. Lumsden, Y. Yiu, J. Knolle, S. Bhattacharjee, D. L. Kovrizhin, R. Moessner, D. A. Tennant, D. G. Mandrus, and S. E. Nagler, Nat. Mater. **15**, 733 (2016).

[3] N. P. Armitage, Nat. Mater. **15**, 701 (2016).

[4] A. Kitaev, Ann. Phys. **321**, 2 (2006).

[5] S. K. Choi, R. Coldea, A. N. Kolmogorov, T. Lancaster, I. I. Mazin, S. J. Blundell, P. G. Radaelli, Yogesh Singh, P. Gegenwart, K. R. Choi, S.-W. Cheong, P. J. Baker, C. Stock, and J. Taylor, Phys. Rev. Lett. **108**, 127204 (2012).

[6] Y. Singh, S. Manni, J. Reuther, T. Berlijn, R. Thomale, W. Ku, S. Trebst, and P. Gegenwart, Phys. Rev. Lett. **108**, 127203 (2012).

[7] R. Comin, G. Levy, B. Ludbrook, Z.-H. Zhu, C. N. Veenstra, J. A. Rosen, Yogesh Singh, P. Gegenwart, D. Stricker, J. N. Hancock, D. van der Marel, I. S. Elfimov, and A. Damascelli, Phys. Rev. Lett. **109**, 266406 (2012).

[8] G. Cao, T. F. Qi, L. Li, J. Terzic, V. S. Cao, S. J. Yuan, M. Tovar, G. Murthy, and R. K. Kaul, Phys. Rev. B **88**, 220414 (2013).

[9] F. Ye, S. Chi, H. Cao, B. C. Chakoumakos, J. A. Fernandez-Baca, R. Custelcean, T. F. Qi, O. B. Korneta, and G. Cao, Phys. Rev. B **85**, 180403 (2012).

[10] X. Liu, T. Berlijn, W.-G. Yin, W. Ku, A. Tsvelik, Young-June Kim, H. Gretarsson, Yogesh Singh, P. Gegenwart, and J. P. Hill, Phys. Rev. B **83**, 220403 (2011).

[11] S. C. Williams, R. D. Johnson, F. Freund, Sungkyun Choi, A. Jesche, I. Kimchi, S. Manni, A. Bombardi, P. Manuel, P. Gegenwart, and R. Coldea, Phys. Rev. B **93**, 195158 (2016).

[12] L. J. Sandilands, Y. Tian, K. W. Plumb, Y.-J. Kim, and K. S. Burch, Phys. Rev. Lett. **114**, 147201 (2015).

[13] A. Koitzsch, C. Habenicht, E. Müller, M. Knupfer, B. Büchner, H. C. Kandpal, J. van den Brink, D. Nowak, A. Isaeva, and Th. Doert, Phys. Rev. Lett. **117**, 126403 (2016).

[14] K. W. Plumb, J. P. Clancy, L. J. Sandilands, V. V. Shankar, Y. F. Hu, K. S. Burch, H.-Y. Kee, and Y.-J. Kim, Phys. Rev. B **90**, 041112 (2014).
[15] G. Jackeli and G. Khaliullin, Phys. Rev. Lett. **102**, 017205 (2009).
[16] J. Chaloupka, G. Jackeli, and G. Khaliullin, Phys. Rev. Lett. **105**, 027204 (2010).
[17] J. Knolle, D. L. Kovrizhin, J. T. Chalker, and R. Moessner, Phys. Rev. Lett. **112**, 207203 (2014).
[18] H. B. Cao, A. Banerjee, J. Q. Yan, C. A. Bridges, M. D. Lumsden, D. G. Mandrus, D. A. Tennant, B. C. Chakoumakos, and S. E. Nagler, Phys. Rev. B **93**, 134423 (2016).
[19] J. A. Sears, M. Songvilay, K. W. Plumb, J. P. Clancy, Y. Qiu, Y. Zhao, D. Parshall, and Y.-J. Kim, Phys. Rev. B **91**, 144420 (2015).
[20] F. Lang, P. J. Baker, A. A. Haghighirad, Y. Li, D. Prabhakaran, R. Valentí, and S. J. Blundell, Phys. Rev. B **94**, 020407 (2016).
[21] J. P. Perdew, K. Burke, and M. Ernzerhof, Phys. Rev. Lett. **77**, 3865 (1996).
[22] P. E. Blochl, Phys. Rev. B **50**, 17953 (1994).
[23] A. I. Liechtenstein, V. I. Anisimov, and J. Zaanen, Phys. Rev. B **52**, R5467 (1995).
[24] L. J. Sandilands, Y. Tian, A. A. Reijnders, H.-S. Kim, K. W. Plumb, Y.-J. Kim, H.-Y. Kee, and K. S. Burch, Phys. Rev. B **93**, 075144 (2016).
[25] K. Foyevtsova, H. O. Jeschke, I. I. Mazin, D. I. Khomskii, and R. Valentí, Phys. Rev. B **88**, 035107 (2013).
[26] B. J. Kim, H. Jin, S. J. Moon, J.-Y. Kim, B.-G. Park, C. S. Leem, J. Yu, T. W. Noh, C. Kim, S.-J. Oh, J.-H. Park, V. Durairaj, G. Cao, and E. Rotenberg, Phys. Rev. Lett. **101**, 076402 (2008).
[27] H.-S. Kim, V. V. Shankar, A. Catuneanu, and H.-Y. Kee, Phys. Rev. B **91**, 241110 (2015).
[28] S. Sinn, C. H. Kim, B. H. Kim, K. D. Lee, C. J. Won, J. S. Oh, M. Han, Y. J. Chang, N. Hur, H. Sato, B. G. Park, C. Kim, H. Kim, and T. W. Noh, Sci. Rep. **6**, 39544 (2016).
[29] B. H. Kim, T. Shirakawa, and S. Yunoki, Phys. Rev. Lett. **117**, 187201 (2016).
[30] S. Agrestini, C.-Y. Kuo, K.-T. Ko, Z. Hu, D. Kasinathan, H. Babu Vasili, J. Herrero-Martin, S. M. Valvidares, E. Pellegrin, L.-Y. Jang, A. Henschel, M. Schmidt, A. Tanaka, and L. H. Tjeng, arXiv:1704.05100.
[31] C. H. Sohn, H.-S. Kim, T. F. Qi, D. W. Jeong, H. J. Park, H. K. Yoo, H. H. Kim, J.-Y. Kim, T. D. Kang, Deok-Yong Cho, G. Cao, J. Yu, S. J. Moon, and T. W. Noh, Phys. Rev. B **88**, 085125 (2013).
[32] M. Shimizu, Rep. Prog. Phys. **44**, 329 (1981).
[33] P. Liu, S. Khmelevskyi, B. Kim, M. Marsman, D. Li, X.-Q. Chen, D. D. Sarma, G. Kresse, and C. Franchini, Phys. Rev. B **92**, 054428 (2015).
[34] H. J. Xiang, S.-H. Wei, M. H. Whangbo, and J. L. F. Da Silva, Phys. Rev. Lett. **101**, 037209 (2008).
[35] P. H. Dederichs, S. Blügel, R. Zeller, and H. Akai, Phys. Rev. Lett. **53**, 2512 (1984).
[36] V. L. Moruzzi, P. M. Marcus, K. Schwarz, and P. Mohn, Phys. Rev. B **34**, 1784 (1986).
[37] P. Kurz, F. Förster, L. Nordström, G. Bihlmayer, and S. Blügel, Phys. Rev. B **69**, 024415 (2004).
[38] P.-W. Ma and S. L. Dudarev, Phys. Rev. B **91**, 054420 (2015).
[39] B. Kaduk, T. Kowalczyk, and T. Van Voorhis, Chem. Rev. **112**, 321 (2011).
[40] G. Kresse and D. Joubert, Phys. Rev. B **59**, 1758 (1999).
[41] O. Bengone, M. Alouani, P. Blöchl, and J. Hugel, Phys. Rev. B **62**, 16392 (2000).
[42] K. Hu, F. Wang, and J. Feng, Phys. Rev. Lett. **115**, 167204 (2015).
[43] Y. Sizyuk, C. Price, P. Wölfle, and N. B. Perkins, Phys. Rev. B **90**, 155126 (2014).
[44] Y. Yamaji, Y. Nomura, M. Kurita, R. Arita, and M. Imada, Phys. Rev. Lett. **113**, 107201 (2014).
[45] S. M. Winter, Y. Li, H. O. Jeschke, and R. Valenti, Phys. Rev. B **93**, 214431 (2016).
[46] J. G. Rau, E. K.-H. Lee, and H.-Y. Kee, Phys. Rev. Lett. **112**, 077204 (2014).
[47] H. J. Xiang, E. J. Kan, S. H. Wei, M. H. Whangbo, and X. G. Gong, Phys. Rev. B **84**, 224429 (2011).
[48] R. Yadav, N. A. Bogdanov, V. M. Katukuri, S. Nishimoto, J. v. d. Brink, and L. Hozoi, Sci. Rep. **6**, 37925 (2016).
[49] K. Hukushima and K. Nemoto, J. Phys. Soc. Jpn. **65**, 1604 (1996).
[50] Y. S. Hou, H. J. Xiang, and X. G. Gong, New J. Phys. **18**, 043007 (2016).
[51] P. S. Wang, W. Ren, L. Bellaiche, and H. J. Xiang, Phys. Rev. Lett. **114**, 147204 (2015).
[52] J. Chaloupka, G. Jackeli, and G. Khaliullin, Phys. Rev. Lett. **110**, 097204 (2013).
[53] W. Pauli, Zeit. Physik **43**, 601 (1927).
[54] S. Toth and B. Lake, J. Phys.: Condens. Matter **27**, 166002 (2015).